Int. J. Electrochem. Sci., 15 **(2020)** 7531 – 7544, doi: 10.20964/2020.08.95

International Journal of ELECTROCHEMICAL SCIENCE
www.electrochemsci.org

Effect of Deformation and Heat Treatment on Pitting Corrosion Behavior of 7050 Al Alloy

Yao Yao[1], Guofeng Li[1], Jiaxin Tang[1], Wenying Xiong[3], Tianqi Chen[1], Zhifeng Wang[2], Hui Yu[2], Hanqing Xiong[1,]*

[1] Department of Mechanical and Electronic Engineering, Changsha University, Changsha 410022, China
[2] School of Materials Science and Engineering, Hebei University of Technology, Tianjin 300130, China
[3] Hunan Key Laboratory of Advanced Aerospace Materials, Changsha 410205, China
[*]E-mail: xhanqing@163.com

Received: 4 April 2020 / *Accepted:* 5 June 2020 / *Published:* 10 July 2020

Microstructure and pitting corrosion behavior of 7050 Al alloy under hot rolling, solution treating and aging conditions were investigated through optical microscopy, scanning electron microscope, transmission electron microscope, electrochemical measurements and 3D laser scanning microscope. The results show the as-rolled alloy exhibits an incomplete recrystallized microstructure with high dislocation density, while the solution treated alloy presents a complete recrystallized microstructure. The aging treatment leads to the formation of η' and η precipitates, and AlCuFe intermetallics always remain in 7050 Al alloy under deformation and heat treatment conditions. The electrochemical activity increases in the following order: solution-treated alloy < aging-treated alloy < as-rolled alloy, while the corrosion resistance increases in the reverse order. Potentiostatic polarization test demonstrates that the as-rolled alloy possesses higher susceptibility to pitting and faster propagation rate. Effects of microstructure on pitting formation are discussed in detail in this work.

Keywords: 7050 alloy; Pitting Corrosion; Microstructure; Hot rolling; Heat treatment

1. INTRODUCTION

In the field of aircraft, automobile and rail transit, the weight reduction has always been the goal that scientists pursue all over the world. Al alloys are dominant in the light weight design of structure materials because of high strength, excellent processability and low cost [1]. 7050 Al alloy is mainly alloyed with Zn, Mg and Cu elements, and is a heat treatment strengthening alloy. Through optimizing the heat treatment to regulate Mg in combination with Zn to form the key strengthening phase $MgZn_2$ (η' or η), 7050 Al alloy can exhibit an ultra-high strength and good fracture toughness [2, 3]. However, the strength of 7050 Al alloy increases at the expense of decreased corrosion resistance and ductility

normally. In addition, 7050 Al alloy products need plastic deformation, such rolling, forging and extrusion. During the above deformation processes, dislocation, lattice distortion and vacancy are introduced, which have a hugely detrimental impact on corrosion resistance of 7050 Al alloy. The non-uniform plastic deformation even causes annulment to subsequent heat treatment [4]. Consequently, 7050 alloy, like other commercial Al alloys, are also faced with problems of pitting corrosion, intergranular corrosion (IGC), exfoliation corrosion (EXCO) and stress corrosion cracking (SCC) [5-8].

The corrosion types have a heavy dependence on composition, grain structure and precipitates of Al alloys processed by plastic deformation and heat treatment. The presence of impurities, such as Fe and Si, usually results in a localized corrosion due to galvanic interaction [9], thus the control of elemental impurities can improve corrosion resistance of 7050 alloy. Furthermore, Sun et al. [10] found that the more sub-grains were beneficial to the corrosion resistance, while the decrease of the grain size was adverse. Song et al. [11] reported that the EXCO resistance of 7050-T6 alloy was improved with the decreasing quench transfer time and the EXCO susceptibility was significantly affected by the distribution of precipitates at grain boundaries. Krishnan et al. [12] developed a novel aging technique avoiding the loss of solutes at grain boundaries to increase volume fraction of precipitates and to improve the SCC resistance of 7050 alloy. Hou et al. [13] used a high-temperature homogenization treatment to reduce the holding time of 7050 alloy, which also decreased the IGC depth. Actually, pitting corrosion is regarded as the precarious form of corrosion in Al-alloys [14-16], because it is the initial point of other corrosion. The trouble is that it cannot be directly detected and predicted by conventional morphology and electrochemical characterization methods [5].

In this study, microstructures of 7050 Al alloy under deformation and heat treatment conditions were observed and investigated. Pitting corrosion behaviors and morphologies of the alloy were evaluated, and moreover the effect of microstructure on pitting formation was discussed in detail.

2. EXPERIMENTAL

2.1. Materials preparation

The as-received 7050 alloy plate with the thickness of 75 mm used in this study was provided by YUNAN ALUMINUM Co. LTD, and the chemical composition was listed in Table 1. The alloy plate was subjected to hot rolling at 473℃ to achieve 2 mm sheets. The alloy sheet were solution treated at 540°C for 1h and then quenched in water. Then, the solution-treated sheet was artificial-aged at 125°C for 24h. As-rolled, solution-treated and aging-treated samples were used for microstructure observation and electrochemical tests.

Table 1. The chemical composition of as-received 7050 alloy thick plate (wt.%)

Zn	Mg	Cu	Zr	Mn	Fe	Si	Al
5.95	2.25	2.1	0.09	0.02	0.06	0.03	Bal.

2.2. Microstructure analysis

The microstructure of experimental samples was observed by optical microscopy (OM, MJ42, Mshot), scanning electron microscope (SEM, Hitachi, SU1500) and transmission electron microscope (TEM, FEI, Tecnai G2 20). For OM observation, the samples under conditions were ground and polished, then etched with a Keller reagent. The samples for SEM observation were ground and polished, then cleaned directly with absolute ethyl alcohol in an ultrasonic cleaning machine. The samples for TEM analysis were mechanically ground to a thickness of 80 μm and then thinned by twin-jet electropolishing with the solution of 25% nitric acid and 75% methyl alcohol at -25°C.

2.3. Electrochemical measurements

Electrochemical tests were performed by an Adminal electrochemical system (Squidstat Plus, USA) with the typical three electrode comprised of an Ag/AgCl electrode as the reference electrode, a platinum plate with a dimension of 4 × 4 × 0.2mm as the counter electrode, and 1 cm^2 of the alloy as the working electrode. All tests used 0.001 $mol \cdot L^{-1}$ NaCl solution as the electrolyte. Open circuit potentials (OCP) were achieved after an immersion in the electrolyte for 30 min. Potentiodynamic polarization tests were carried out and the testing range from -200 mV to 600 mV with respect to OCP at a scanning rate of 1 $mV \cdot s^{-1}$. After the samples were immersed in the electrolyte for achieving a stable OCP, electrochemical impedance spectroscopy (EIS) was measured at the OCP from 100 kHz to 0.05 Hz with the voltage amplitude of 5 mV.

2.4 Pitting corrosion behavior evaluation

The three electrode system was also employed to evaluate pitting corrosion behaviors of experimental samples. To improve the detection precision, the samples were ground with emery 5000 grit papers, then were polished and cleaned with absolute ethyl alcohol. Potentiostatical polarization tests were used at -600mV (vs Ag/AgCl) for 300 min. Furthermore, the corroded surfaces were estimated with a 3D laser scanning microscope (Keyence VK-X100, Keyence, Japan). The morphology, number, depth, area and volume of pits were systematically analyzed.

3. RESULTS AND DISCUSSION

3.1 Microstructure

The optical microstructures of 7050 alloy under different conditions are illustrated in Fig. 1. For the as-rolled alloy, elongated and recrystallized grains are observed in Fig. 1a. Due to the effect of heat and deformation force, dynamic recovery and recrystallization occur in the alloy during the hot rolling. Fig. 1b shows coarse grains implying that the solution treated alloy is recrystallized completely and then grains grow up. After the aging treatment, it difficult to identify the grain structure, while the

precipitation of secondary phases is obviously viewed in consideration of numerous black particles on Fig.1c. In order to better distinguish impurities, Fig. 2 gives backscattered electron (BSE) images of experimental samples. Obviously, the alloys in different states contain similar intermetallics. Moreover, the major elements including Al, Cu and Fe are detected by EDS results in inset images in Fig.2a, b and c, which indicates one kind of irregular constituent AlCuFe intermetallics [17]. The intermetallic has obvious characteristics, such as the mean equivalent diameter of 1.7 μm, the number density of 220 mm^{-2} and paralleling to the rolling direction [9], it however is very difficult to dissolve in Al matrix during solution treating.

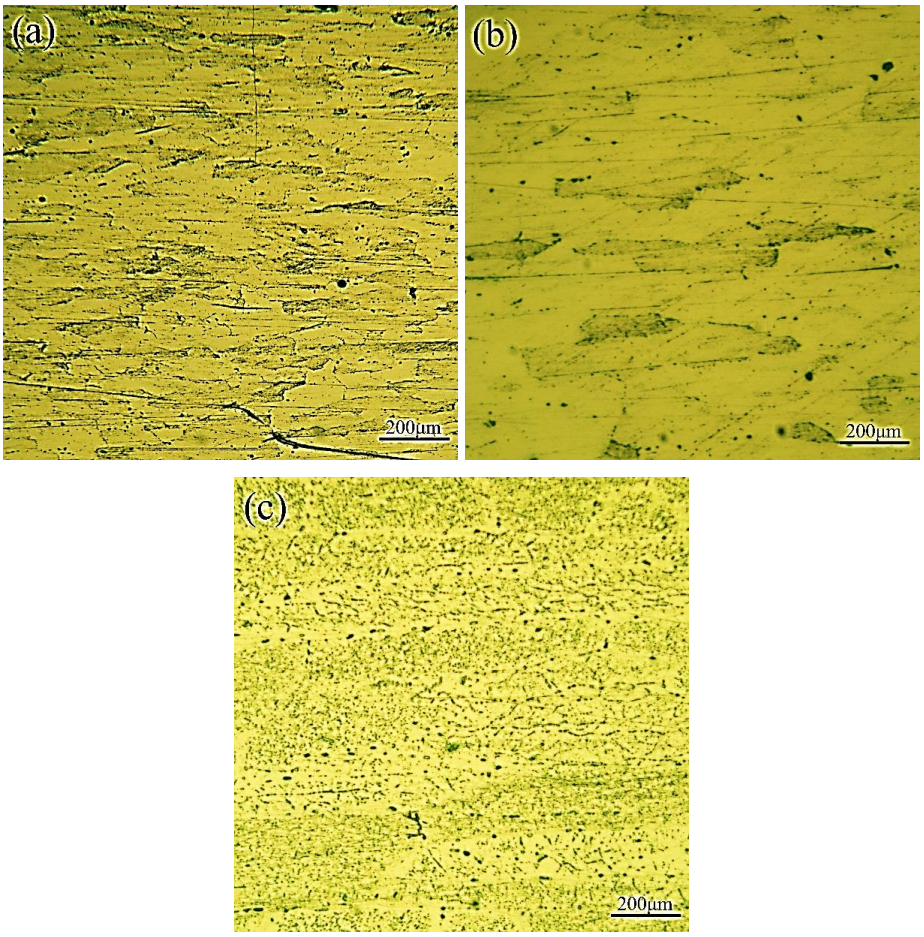

Figure 1. Optical microstructures of 7050 alloy in different states, (a) as-rolled alloy, (b) solution-treated alloy and (c) aging-treated alloy.

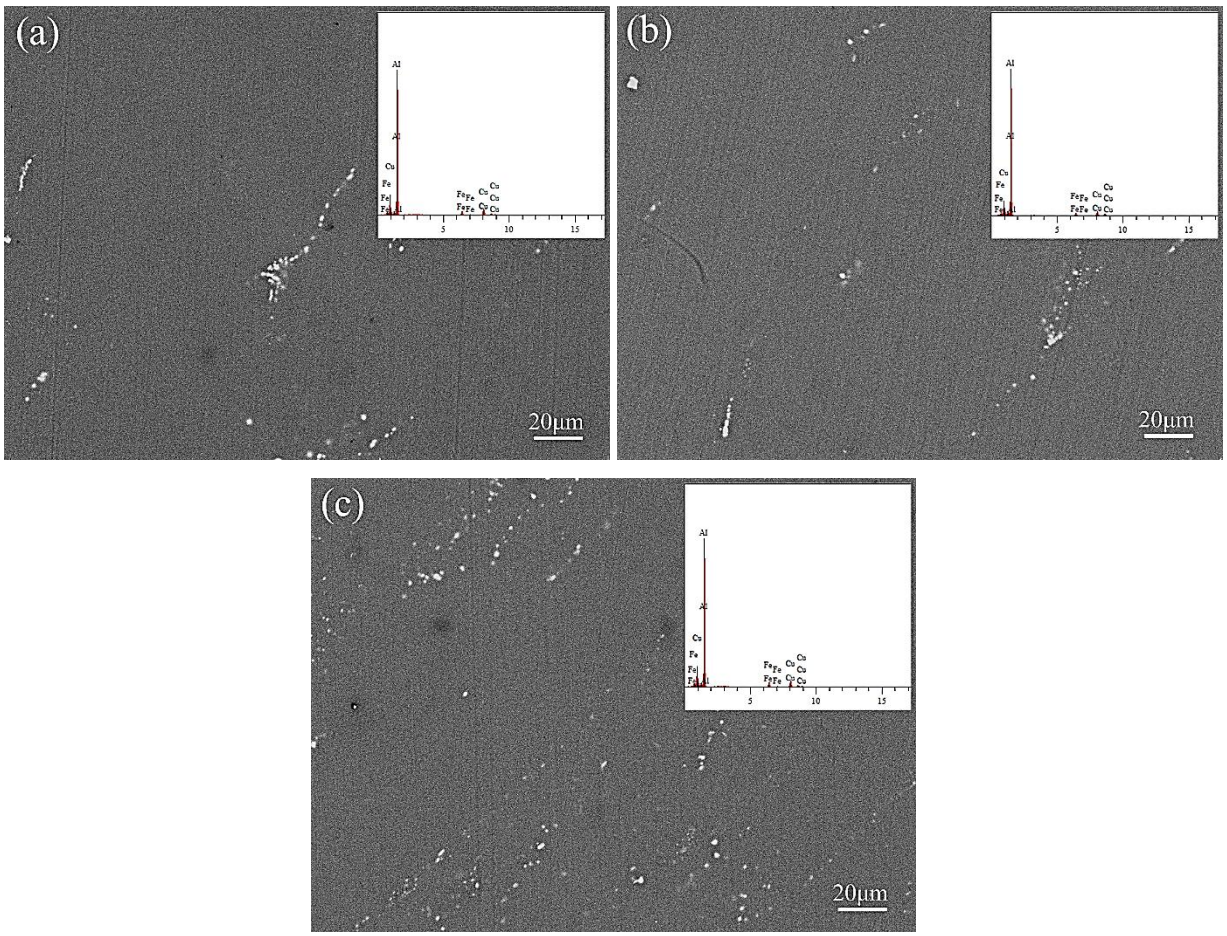

Figure 2. The backscattered electron (BSE) images of 7050 alloy in different states, (a) as-rolled alloy, (b) solution-treated alloy, and (c) aging-treated alloy.

The microstructure characteristics of the alloy under deformation and heat treatment conditions are furthermore revealed by TEM observation viewed along [001] zone axis in Fig. 3. As shown in Fig. 3a, a lot of dislocations accumulated in the as-rolled sample except dynamic recrystallization grains and large grains, which is also prone to an incomplete recrystallization during hot rolling. The solution treated sample exhibits clear grain boundaries in Fig. 3b, and the density of dislocations is reduced at the same time. Fig. 3c displays very fine intragranular precipitates which uniformly distribute in the matrix of the aging-treated sample. In view of corresponding selection area diffraction (SAED) pattern, it indicates the metastable η' phase during aged Al-Zn-Mg(-Cu) alloys and has the semi-coherent relation to the Al matrix [12, 18]. In addition, it is clear from Fig. 3d that both coarse η grain boundary precipitates (GBPs) and precipitate free zones (PFZs) are formed as well.

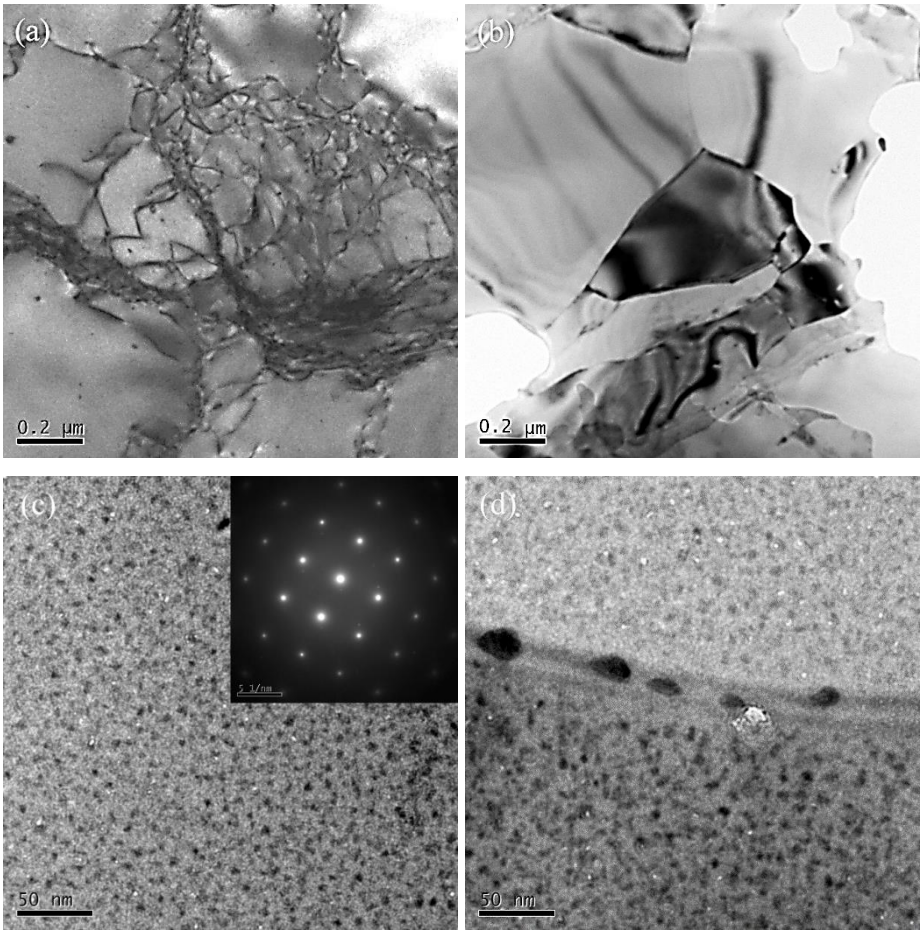

Figure 3. The TEM images of 7050 alloy under different conditions, (a) as-rolled alloy, (b) solution-treated alloy, and (c) aging-treated alloy (intragranular precipitates, corresponding SAED pattern taken from [001] zone axis), and (d) aging-treated alloy (grain boundary precipitates).

3.2 Electrochemical measurement

Fig. 4 shows polarization curves of 7050 alloy under different conditions, and related corrosion parameters are listed in Table 2. Obviously, the corrosion potential (E_{corr}) value decreases in the following order: solution-treated alloy > aging-treated alloy > as-rolled alloy. E_{corr} usually can evaluate electrochemical activity of Al alloys, and moreover the lower negative E_{corr} indicates the higher electrochemical activity which presents the smaller corrosion resistance and more sensitive to corrosion in testing medium [7]. Thus, the electrochemical activity of experimental alloys increases in the following order: solution-treated alloy < aging-treated alloy < as-rolled alloy. For the as-rolled alloy, the lowest E_{corr} is exhibited in this work due to the microstructure evolution during multi-pass hot rolling. Concretely, AlCuFe intermetallics occur in Fig. 2a, the grains are refined in Fig. 1a, and the dislocation density is increased in Fig. 3a. AlCuFe intermetallic has higher corrosion potential compared with Al matrix, and is regarded as the nasty cathode in Al alloys [9, 19, 20]. Consequently, the occurrence of AlCuFe compounds enhances the electrochemical activity of the as-rolled alloy. With grain refining, the number and the area of grain boundaries are increased providing more electrochemical reaction channels

for self-corrosion [21, 22]. Li [23] indicated that in Al-Zn-Mg-Cu alloy, the amount of recrystallized grains at the grain boundaries resulting in aggravating corrosion, while Sun [10] found that the decreased grain size had a detrimental effect on the corrosion resistance. Furthermore, Brunner et al. [24] revealed that the dislocation accumulation was harmful for the corrosion resistance of Al alloys. With the increasing dislocation density during the process of plastic deformation, the corrosion property of Al alloys reduces [25, 26]. Thus, grain refinement and dislocation accumulation also play an important role in the electrochemical activity of the as-rolled alloy. In the aging-treated alloy, a number of η' and η precipitates are formed though the accumulated dislocations are removed, as shown Fig. 3c and d. These precipitates have a lower E_{corr} than the matrix of Al-Zn-Mg-Cu alloy, and especially coarsen GBPs can accelerate anodic dissolution and hydrogen effects leading to the formation of critical defects [7, 27, 28]. As a result, the aging-treated alloy exhibits poor corrosion resistance. In view of the microstructure analysis in solution-treated alloy, it has only AlCuFe compounds as the predominant factor on the corrosion resistance and possesses the weakest electrochemical activity in this test. The J_{corr} (corrosion current density) acquired by Tafel extrapolation decreases in the following order: as-rolled alloy > aging-treated alloy > solution-treated alloy. In addition, a trend of pitting corrosion is observed for the three samples obviously in Fig. 4a, which means the corrosion process of 7050 alloy under different conditions is greatly depending on microstructure characteristics. The pitting corrosion also is related to the dissolution reaction ($Al \rightarrow Al^{3+} + 3e^-$) of Al alloys [12], thus the anodic slope (b_a) can be used to reflect the developing trend of pitting corrosion. Both as-rolled and solution-treated alloys possess similar b_a values because AlCuFe compound is the initial point of pitting corrosion. However, the aging-treated alloy shows higher b_a value than the other two ones due to more η' and η phases, which enhance the initial kinetic of dissolution reaction.

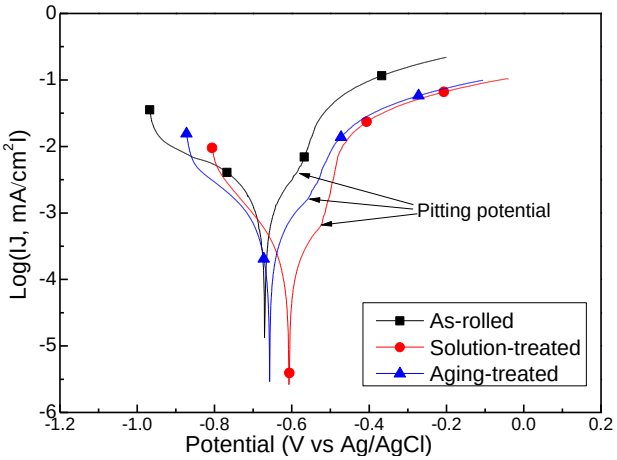

Figure 4. Polarization curves of as-rolled alloy, solution-treated alloy and aging-treated alloy in 0.001 mol·L^{-1} NaCl solution.

Table 2 Corrosion parameters of experimental alloys in 0.001 mol·L^{-1} NaCl solution.

Alloys	E_{corr}/V(vs Ag/AgCl)	j_{corr}/(mA·cm^{-2})	Pitting potential/V(vs Ag/AgCl)	b_a, mV dec^{-1}
As-rolled	-0.670	1.63×10^{-4}	-0.588	23.9 ± 0.5
Solution-treated	-0.607	6.46×10^{-5}	-0.528	23.7 ± 0.5
Aging-treated	-0.650	1.02×10^{-4}	-0.556	27.9 ± 0.5

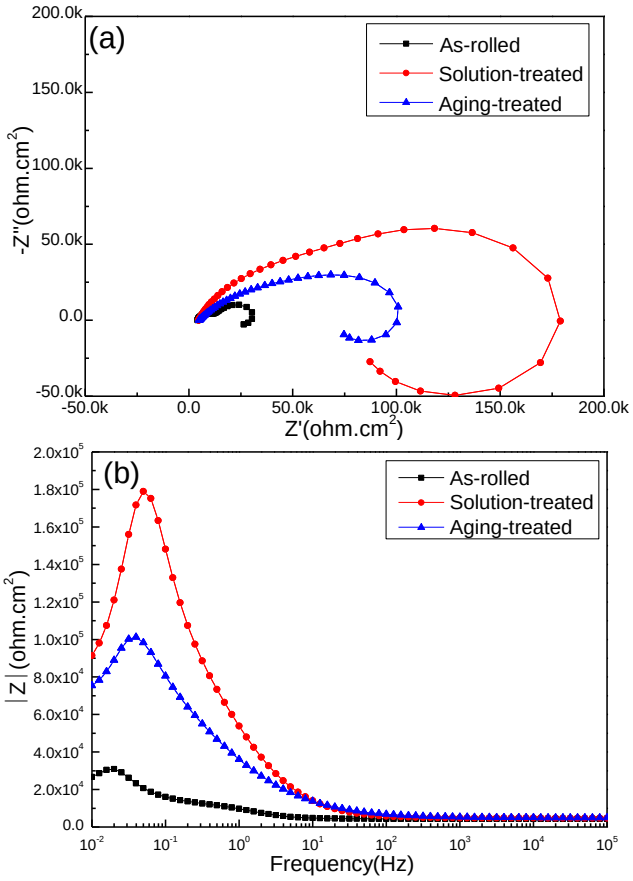

Figure 5. Nyquist plots (a) and Bode plots (b) of as-rolled alloy, solution-treated alloy and aging-treated alloy in 0.001 mol·L^{-1} NaCl solution.

Nyquist and Bode plots of experimental samples are depicted in Fig.5. For the three samples, the similar features of Nyquist plots are observed including two capacitive loops and one inductive capacitive loop from high to low frequency range. The capacitive loop at high frequency range is defined as the electric double layer at the alloy/electrolyte interface related to charge transfer reaction, the capacitive loop at intermediate frequency reflects a complex oxide layer, while the inductive loop is often attributed to the initiation of corrosion [29, 30]. To refine the analysis of circuit models and experimental results, a constant phase element (CPE, impure capacitance) is introduced during fitting process. The impedance of CPE is described with the following formula [30-32]:

$$Z_{CPE} = \frac{1}{Y_0(jw)^n} \quad (1)$$

where Y_0, ω and j represent the CPE-constant, the angular frequency (ω=2πf, f is the frequency) and the imaginary unit, respectively. Moreover, the range of n is from 0 to 1, which can express an ideal

capacitance CPE with heterogeneous effects. On the basis of the assumption, the corresponding equivalent circuits are displayed in Fig. 6 and subsequently the data fitted by Zsimpwin software 3.3 are listed in Table 3.

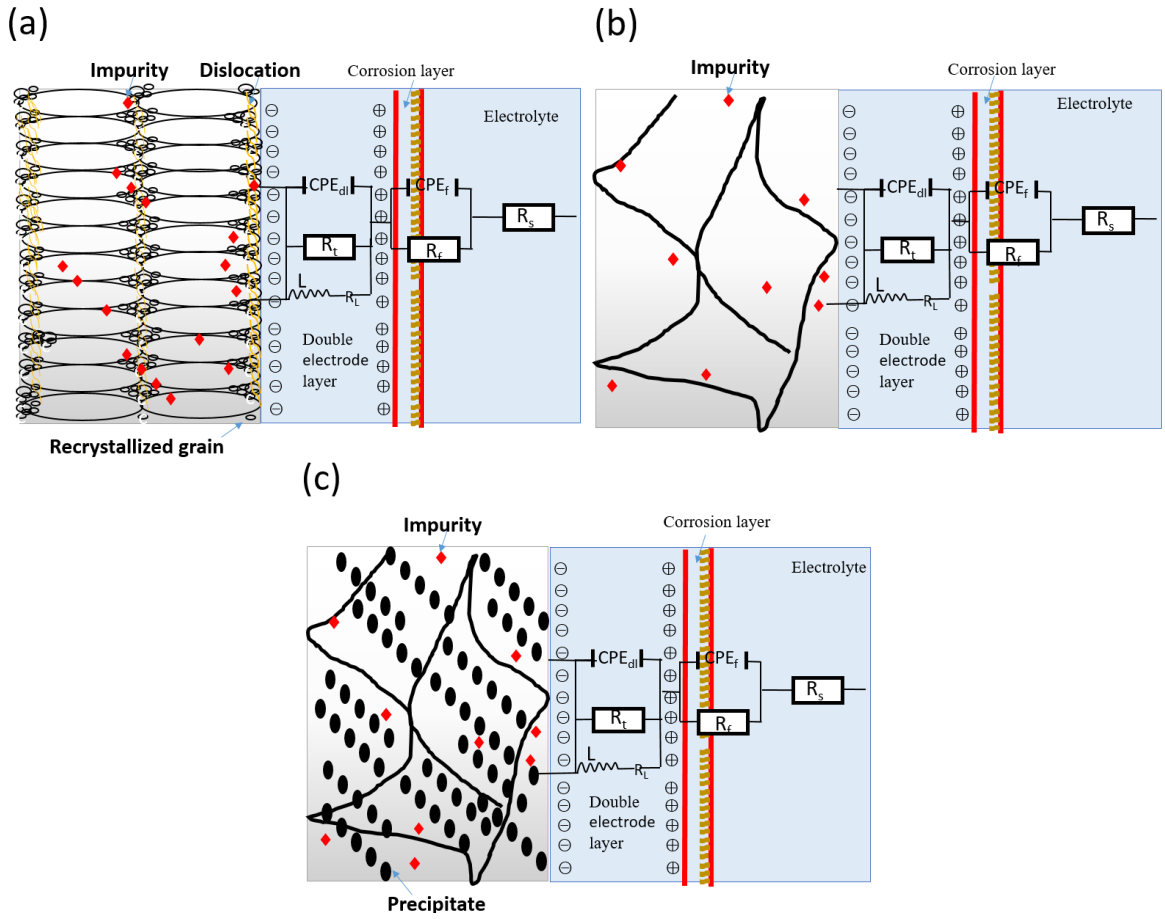

Figure 6. Equivalent circuits of 7050 alloy under different conditions corresponding to the EIS results, (a) as-rolled alloy, (b) solution-treated alloy, and (c) aging-treated alloy.

In Fig. 6, R_t, R_f, R_L and R_s represent the charge transfer resistance, the solution resistance, the resistance of oxide layer and pseudo resistance respectively; CPE_{dl} and CPE_f indicate the capacitance alloy/electrolyte interface and the capacitance of oxide layer respectively; L is a pseudo inductance, which can combine with R_L partially reflecting the breakdown of oxide layer and the formation of new corrosion interface [32, 33].

Table 3. EIS simulated values of 7050 alloy in different states.

Alloy samples	As-rolled	Solution-treated	Aging-treated
R_s ($\Omega \cdot cm^2$)	4301	4723	4876
CPE_{dl} ($\Omega^{-1} \cdot cm^{-2} \cdot s^n$)	2.05×10^{-4}	4.031×10^{-6}	8.25×10^{-6}

n_1 ($0 < n < 1$)	1	0.7635	0.5948
R_t ($\Omega \cdot cm^2$)	2.117×10^4	7.501×10^4	6.859×10^4
CPE_f ($\Omega^{-1} \cdot cm^{-2} \cdot s^n$)	2.188×10^{-5}	1.619×10^{-5}	4.854×10^{-5}
n_2 ($0 < n < 1$)	0.8884	0.8978	0.8143
R_f ($\Omega \cdot cm^2$)	8298	1.15×10^5	4.589×10^4
L($H \cdot cm^2$)	1.617×10^5	4.93×10^5	2.509×10^5
R_L	1972	7286	6891
χ^2	1.45×10^{-4}	2.30×10^{-3}	2.80×10^{-3}

The corrosion process of 7050 alloy under different conditions can be explained on the basis of the equivalent circuits in Fig. 6. It is obvious that the corrosion resistance of experimental samples is significantly related to R_t, R_f and R_L. Firstly, R_t can give expression to the electrochemical activity because the exchange current is directly associated with the corrosion process of experimental alloys [34]. Secondly, R_f can cause obstacle to the progress of exchange transfer since the passivation of Al alloys in a water-air-containing medium [34]. Finally, R_L and L are determined by microstructure characteristics of Al alloys [35], which can be conducive to corrosion defects and the progress of corrosion. Through Bode plots of impedance modulus (|Z|) vs frequency, the |Z| value decreases in the order: solution-treated alloy > aging-treated alloy > as-rolled alloy. For the as-rolled alloy in this work, the smallest |Z| value is attributed to impurities, dislocations and fine dynamically recrystallized grains. The solution-treated alloy presents the largest |Z| value only affected by impurities. Compared with that of the as-rolled alloy, the |Z| value of the aging-treated alloy becomes larger due to the reduced dislocation density and the increased precipitates.

3.3 Pitting corrosion tests

Fig. 7 shows potentiostatic polarization process of 7050 alloy in different states at -600 mV, and the tendency of current densities is revealed from 0 to 300 min. Obviously, the solution-treated and aging-treated samples demonstrate a relatively slow current rise, which implies a stable pitting progress during testing process below the pitting potential. The oxide layer on the solution-treated and aging-treated alloys has a high stability during the potentiostatic polarization process. Furthermore, the current density of the aging-treated alloy is slightly larger than that of the solution-treated one on account of more precipitates. The slow current rise also is attributed to the relative homogeneity of precipitates in the aging-treated alloy. For the as-rolled alloy, the curve of current density shows a current plateau first and then increases rapidly after 30 min, suggesting the occurrence of excessive pitting with time extension. The phenomenon also is ascribed to impurities, dislocations and fine dynamically recrystallized grains, which cause inhomogeneity in the microstructure of the as-rolled alloy.

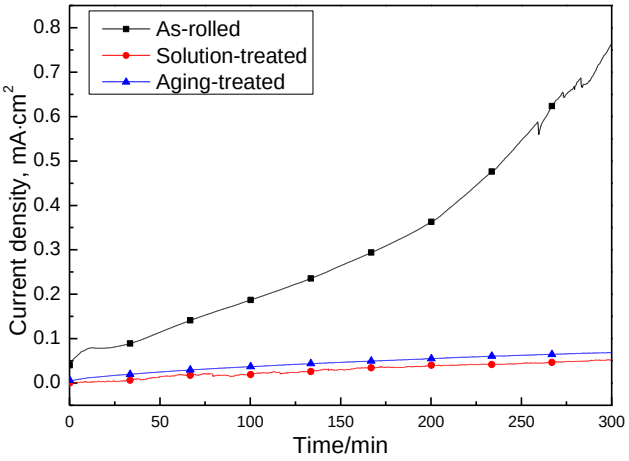

Figure 7. Potentiostatic polarization process of as-rolled alloy, solution-treated alloy and aging-treated alloy at -600 mV in 0.001 mol·L^{-1} NaCl solution.

Pitting morphologies and three-dimensional geometric data of 7050 alloys under different conditions are presented in Fig. 8. It can be seen that the three samples present different pitting characteristics. In view of the number, the area and the volume of pits, the as-rolled sample all exhibits larger values. This illustrates that the as-rolled alloy has lower corrosion resistance and is more likely to be eroded by aggressive anions with respect to the other ones, which is consistent with the electrochemical tested results. For the aging-treated alloy, though the tendency of pitting corrosion is small according to Fig.7, the number of pits is close to that of the as-rolled alloy.

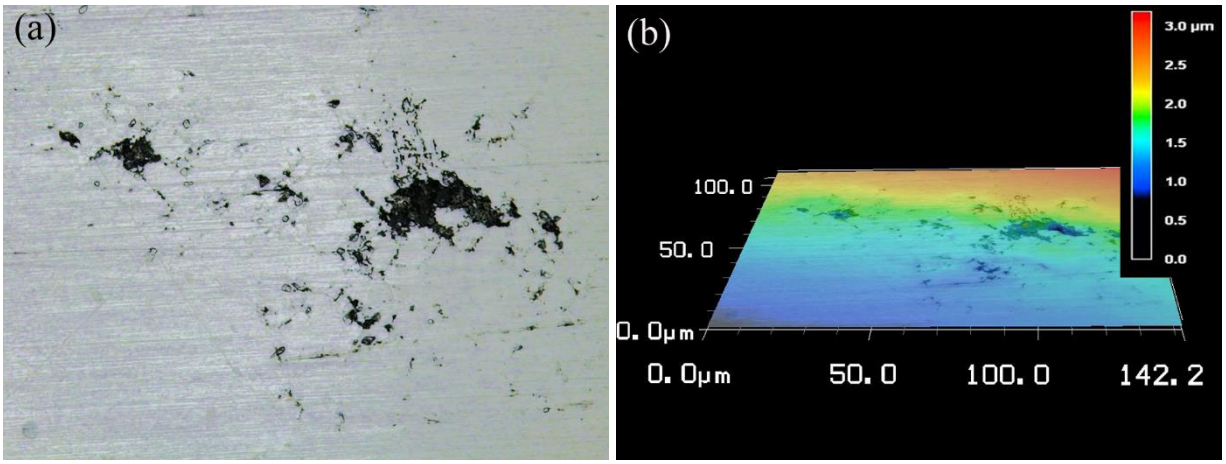

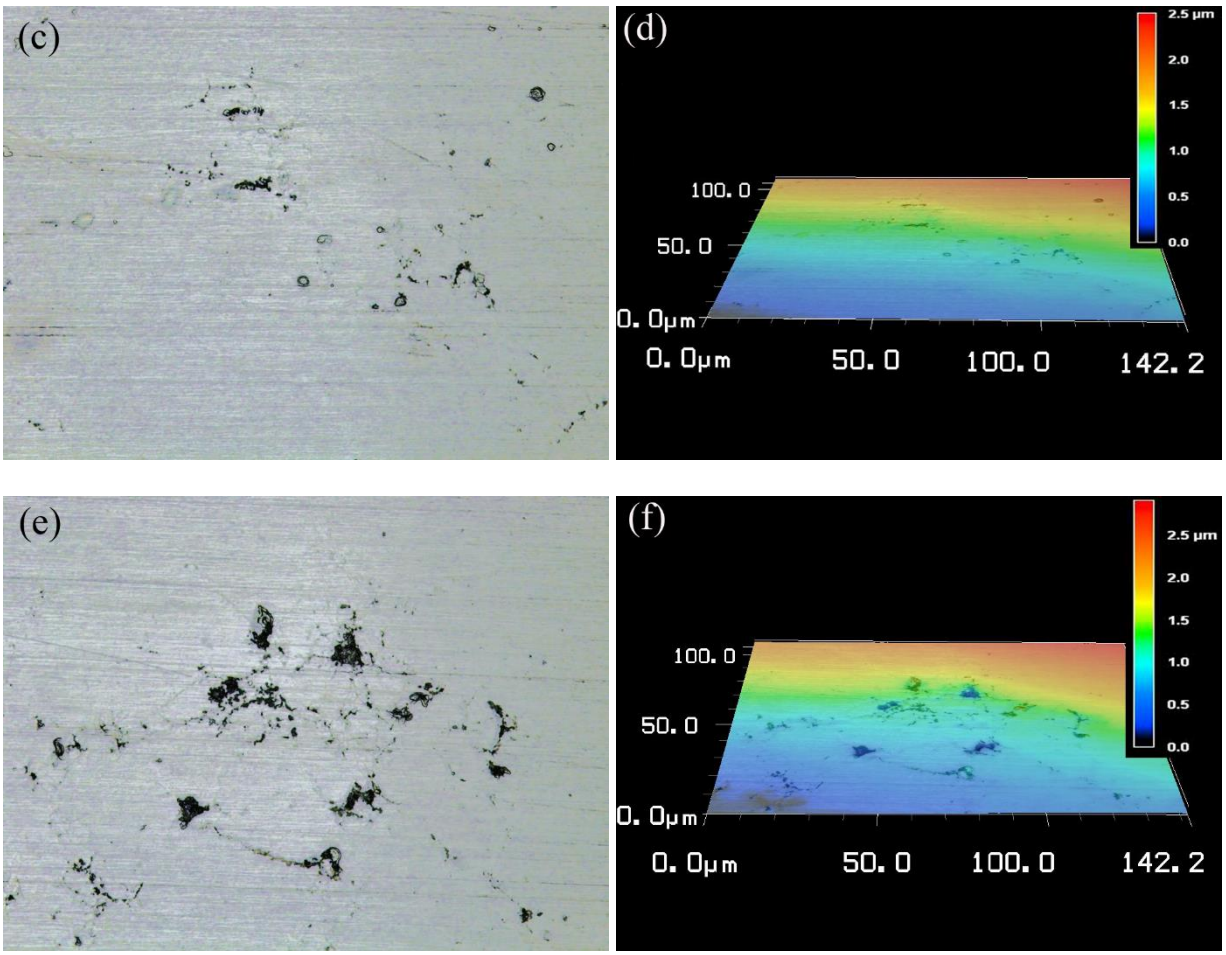

Figure 8. Pitting morphologies of 7050 alloys after potentiostatic polarization for 300 min, (a, b) as-rolled alloy, (c, d) solution-treated alloy and (e, f) aging-treated alloy.

In Al alloys, AlCuFe compound with high E_{corr} can act as the cathode, while η' and η precipitates with low E_{corr} compared is considered as anodes. Through the galvanic effect of AlCuFe compound, Al matrix is corroded. Combined with dislocations and non-uniform recrystallized grains, the degree of localized corrosion is enlarged in as-rolled alloy. However, η' and η precipitates are corroded in the aging-treated alloy through the galvanic effect, the Al matrix is more remained during potentiostatic polarization test due to less dislocations and uniform grains. Furthermore, a few pits are observed in Fig. 8c and d, because the solution-treated alloy is only marginally affected by AlCuFe compound, which also means the solution-treated alloy possesses better pitting corrosion resistance.

4. CONCLUSIONS

The 7050 alloy subjected to hot rolling deformation presents the incomplete recrystallized microstructure with high dislocation density. The solution treatment decreases dislocation density leading to the formation of complete recrystallized microstructure. After the aging treatment, the uniform distribution of η' precipitates is confirmed and coarse η precipitates occur at the grain boundary. During the process of deformation and heat treatment, AlCuFe intermetallics always exist in the alloy.

The electrochemical activity increases in the following order: solution-treated alloy < aging-treated alloy < as-rolled alloy, while the corrosion resistance increases in the reverse order. Moreover, the solution-treated alloy exhibits the best pitting corrosion resistance due to the only effect of AlCuFe intermetallics. The as-rolled alloy possesses higher susceptibility to pitting and faster propagation rate attributed to AlCuFe intermetallics, dislocations and non-uniform recrystallized grains which enlarge the degree of localized corrosion. Compared with the as-rolled alloy, the aging-treated alloy is affected by AlCuFe intermetallics and precipitates, while η' and η act as anodes, Al matrix is more remained.

ACKNOWLEDGE`MENT
This work was financially supported by the Fundamental Research Funds for the Education Department of Hunan Province (17A019). The authors also acknowledge the Project (KC1809018) supported by the science and technology program of Changsha, the outstanding youth project (18B418) of Education Department of Hunan Province, and the Changsha University talent introduction project (50800-93292).

References

1. X. Zhang, Y. Chen, J. Hu, *Prog. Aerosp. Sci.*, 97 (2018) 22.
2. G. Li, X. Zhang, P. Li, J. You, *Trans. Nonferrous Met. Soc. China*, 20 (2010) 935.
3. Y. Wang, Q. Pan, L. Wei L, B. Li, Y. Wang, *Mater. Design*, 55 (2014) 857.
4. X. Zhang, X. Zhou, T. Hashimoto, B. Liu, C. Luo, Z. Sun, Z. Tang, F. Lu, Y. Ma, *Corros. Sci*., 132 (2018) 1.
5. A. Nicolas, A. Mello, M. Sangid, *Corros. Sci*., 154 (2019) 208.
6. Z. Zhao, H. Zhang, Y. Li, X. Chen, Y. Liu, *Corros. Eng. Sci. Techn.*, 54 (2019) 122.
7. J. Chen, X. Zhang, L. Zou, Y. Yu, Q. Li, *Mater. Charact.*, 114 (2016) 1.
8. G. Özer, I. Kaya, A. Karaaslan, *Mater. Corros.*, 70 (2019) 1788.
9. J. Li, J. Dang, *Metals*, 7 (2017) 84.
10. L. Sun, M. Chen, Y. Deng, *Int. J. Mod. Phys. B*, 33 (2019) 1940011.
11. F. Song X, X. Zhang, S. Liu, Q. Tan, D. Li, *Trans. Nonferrous Met. Soc. China*, 24 (2014) 2258.
12. M. Krishnan, V. Raja, S. Shukla, S. Vaidya, *Metall. Mater. Trans. A*, 49 (2018) 2487.
13. W. Hou, W. Ji, Z. Zhang, J. Xie, X. Cheng, *J. Mater. Process. Tech.*, 214 (2014) 635.
14. M. Naeini, M. Shariat H, M. Eizadjou, *J. Alloy Comp*., 509 (2011) 4696.
15. Z. Li, S. Lv, X. Gao, T. Srivatsan, *Emerg. Mater. Res.*, 8 (2019) 206.
16. B. Zhang, X. Ma, *J. Mater. Sci. Technol.*, 35 (2019) 1455.
17. A. Hughes, C. Macrae, N. Wilson, A. Torpy, T. Muster, A. Glenn, *Surf. Interface Anal.*, 42 (2010) 334.
18. A. Ghosh, M. Ghosh, G. Shankar, *Mat. Sci. Eng*. A, 738 (2018) 399.
19. K. Zhao, J. Liu, M. Yu, S. Li, *Trans. Nonferrous Met. Soc. China*, 29 (2019) 1793.
20. A. Boag, A. Hughes E, N. Wilson, A.Torpy, C. MacRae, A. Glenn, T. Muster, *Corros. Sci*., 51 (2009) 1565.
21. Y. Wu, Z. Wang, Y. Liu, G. Li, S. Xie, H. Yu, H. Xiong, *J. Mater. Eng. Perform*., 28(2019) 2006.
22. Y. Wu, Z. Wang, Y. Liu, G. Li, S. Xie, H. Yu, H. Xiong, *Int. J. Electrochem. Sci.*, 13 (2018) 10325.
23. J. Li, F. Li, X. Ma, J. Li, S. Liang, *Mat. Sci. Eng*. A, 732 (2018) 53.
24. J. Brunner, N. Birbilis, K. Ralston, S. Virtanen, *Corros. Sci*., 57 (2012) 209.
25. J. Li, F. Li, J. Li, S. Liang, *Mater. Corros.*, 70 (2018) 234.
26. X. Zhang, Z. Wang, Z. Zhou, J. Cao, G. Yang, *Int. J. Electrochem. Sci.*, 15 (2020) 1727.
27. X. Peng, G. Qi, X. Liang, Y. Deng, Y. Gu, G. Xu, Z. Yin, *Mat. Sci. Eng. A*, 688 (2017) 146.

28. V. Arizmendi-Salgado, S. Serna, A. Torres-Islas, R. Soto-Espitia, P. Althuzer, S. Mejia-Sintillo, J. Campos-Alvarez, J. Gonzalez-Rodriguez, *Int. J. Electrochem. Sci.*, 14 (2019) 8243.
29. L. Feng, Q. Pan, L. Wei, J. Cent. South Univ., 22 (2015) 2423.
30. P. Kanta, V. Srivastava, K. Venkateswarlu, S. Paswan, B. Mahato, G. Das, K. Sivaprasad, K. Krishna, Inter. J. Min. Met. Mater., 24 (2017) 1293.
31. Y. Xiao, Q. Pan, W. Li, X. Liu, Y. He, *Mater. Design*, 32 (2011) 2149.
32. Y. Cheng, Z. Zhang, F. Cao, J. Li, J. Zhang, J. Wang, C. Cao, *Corros. Sci*., 46 (2004) 1649.
33. Chen S, Chen K, Peng G, L. Jia, P. Dong, *Mater. Design*, 35 (2012) 93.
34. J. Brunner, N. Birbilis, K. Ralston, S. Virtanen, *Corros. Sci*., 57 (2012) 209.
35. P. Liu, L. Hu, Q. Zhang, C. Yang, Z. Yu, J. Zhang, J. Hu, F. Cao, *J. Mater. Sci. Technol.*, (2019) doi.org/10.1016/j.jmst.2019.09.030.